Rotation of Single-Molecule Emission Polarization by Plasmonic Nanorods

Tiancheng Zuo[1,+], Harrison J. Goldwyn[2,+], Benjamin P. Isaacoff[1], David J. Masiello[,2], Julie S. Biteen*[,1]*

[1]Department of Chemistry, University of Michigan, Ann Arbor, MI 48109
[2]Department of Chemistry, University of Washington, Seattle, WA 98195
[+]T.Z. and H.J.G. contributed equally to this work
*Correspondence: jsbiteen@umich.edu, masiello@uw.edu

ABSTRACT: The strong light-matter interactions between dyes and plasmonic nanoantennas enable the study of fundamental molecular-optical processes. Here, we overcome conventional limitations with high-throughput single-molecule polarization-resolved microscopy to measure dye emission polarization modifications upon near-field coupling to a gold nanorod. We determine that the emission polarization distribution is not only rotated toward the nanorod's dominant localized surface plasmon mode as expected, but is also unintuitively broadened. With a reduced-order analytical model, we elucidate how this distribution broadening depends upon both far-field interference and off-resonant coupling between the molecular dipole and the nanorod transverse plasmon mode. Experiments and modeling reveal that a nearby plasmonic nanoantenna affects dye emission polarization through a multicolor process, even when the orthogonal plasmon modes are separated by approximately three times the dye emission linewidth. Beyond advancing our understanding of plasmon-coupled emission modifications, this work promises to improve high-sensitivity single-molecule fluorescence imaging, biosensing, and spectral engineering.

Table of Contents Graphic

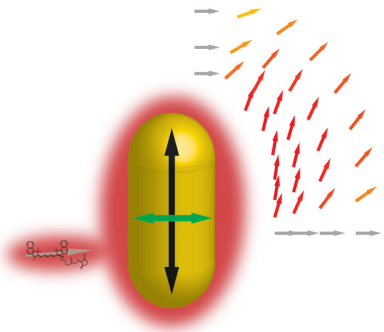

Nanoantennas couple the far field to the near field by converting propagating waves to localized fields.[1] Understanding and measuring how optical nanoantennas couple to their local environment is a critical step toward controlling and enhancing near-field properties for applications as diverse as biosensors,[2,3] light-emitting devices,[4,5] surface-enhanced Raman spectroscopy,[6,7] and super-resolution microscopy.[8-11] Noble metal nanoparticles respond strongly to light and are efficient nanoantennas. Upon optical excitation, localized surface plasmons (LSPs)—collective oscillations of the metal conduction-band electrons—are created at the nanoparticle surface and concentrate radiation into intense near fields through which optical processes in the surrounding local environment can be enhanced.

One intriguing near-field effect of plasmonic nanoparticles is their ability to interact with nearby fluorescent dye molecules. Reported experimental and theoretical studies of the coupling of single dye molecules with metal nanoparticles have described how these nanoantennas modify the rate,[9,12-17] spatial distribution,[10,18,19] spectrum,[14] and polarization[8,20-25] of fluorescence emission. Single-molecule experiments, which avoid ensemble averaging,[10] have further shown that single-molecule fluorescence emission is re-directed by a plasmonic nanoantenna,[26] and recent theory has proposed that this so-called mislocalization can be attributed to the superposition and interference of the molecule and nanoantenna far-field emission as well as to the near-field coupling between the two emitters.[19,27] In general, the excitation and decay of coupled fluorescent molecules and nanoantennas can be treated as separate processes as there is no coherence between plasmon-coupled molecular absorption and emission,[14,28] and experiments have shown that emission mislocalization is independent from enhanced absorption.[26,29]

Despite this research activity, the interaction between nanoantennas and nearby molecules is still not fully understood. Previous studies have demonstrated that emission

polarization of a single emitter can be modified by the orientation of a nearby asymmetric nanoantenna such as a nanorod or Yagi-Uda antenna.[21,23,25] Here, we extend these previous studies by using Points Accumulation for Imaging in Nanoscale Topography (PAINT) experiments[8,31-33] to sample thousands of molecules that transiently adsorb on the coverslip near each antenna. We also explicitly subtract the contribution of plasmonic particle photoluminescence,[34] and develop novel understanding of how this dye-nanoantenna coupling influences the polarization of emitted light by combining single-molecule experiments with a reduced-order analytical model. The model results not only agree with simulation and provide a faster route to polarization prediction, but elucidate the mechanisms underlying emission polarization modification from a coupled dye-antenna system by isolating effects from the nanoantenna's two orthogonal dipole plasmon modes. The model also reveals the contributions to emission polarization from near-field coupling and far-field interference, both of which vary differently with dye-nanoantenna position and orientation.

More specifically, we investigate the polarization changes that result from plasmon-coupled emission by measuring the emission polarization of single dye molecules coupled to individual plasmonic nanorods. By correlating the single-molecule emission polarization angle with the nanorod orientation and fluorescence wavelength, we observe that the molecular emission polarization is significantly rotated toward the angle of the nanoantenna dominant plasmon mode as previously reported,[20-25] and can be as large as 90°. We use single-molecule polarization-resolved microscopy to measure the angle distribution of this "mispolarization" for two different dyes—one red, Cy5.5 (λ_{max} = 710 nm) and one bluer, Cy3 (λ_{max} = 570 nm), and we find that measurable mispolarization occurs even when off resonance from the plasmon. This emission effect is therefore different from the fluorescence intensity and fluorescence emission

spectrum, which are affected by both plasmon-coupled absorption and plasmon-coupled fluorescence emission.[26]

Single-molecule polarization-resolved microscopy. To measure the emission polarization of single dye molecules coupled to gold nanorods, we achieve a sparse distribution of fluorescent molecule detections by placing a drop of nanomolar dye solution over a nanorod-coated coverslip (Fig. 1a). In this PAINT experiment,[8,31-33] most molecules diffuse rapidly in solution and are not detected by the camera (at 10 frames/s); only those molecules that transiently adsorb on the coverslip are captured by the camera. The high magnification of the microscope (160 nm/imaging pixel) and low concentration of dye molecules enable us to characterize one molecule at a time. A polarizing beam displacer (PBD) in the emission pathway of our single-molecule microscope (Fig. 1a) separates the emission into two orthogonally polarized output beams, which are then offset from one another and projected onto the camera (white "Center channel" and "Off-center channel" boxes in Fig. 1a). In this two-channel, one-camera setup, the emission from each single dye molecule appears in two channels (e.g., cyan circles in Fig. 1a), but the intensity is different in each channel. The apparent emission polarization angle, ϕ_{apparent}, of each fluorescent molecule and photoluminescent nanorod is thus related to the intensity ratio recorded in these two channels according to:

$$\phi_{\text{apparent}} = \tan^{-1}\sqrt{\frac{\langle I_{\text{off-center}}\rangle}{\langle I_{\text{center}}\rangle}} \quad (1)$$

where $\langle I_{\text{center}}\rangle$ and $\langle I_{\text{off-center}}\rangle$ are the detected intensities in the center and off-center images, respectively, integrated over a diffraction-limited area. This expression maps all angles into the first quadrant (between 0 and 90°) because phase information is lost from both field components.

Single-molecule polarization-resolved microscopy measures the average emission polarization in the image plane, which corresponds to the physical dipole orientation for isolated single emitters (dye molecules or nanorods) lying flat on the microscope coverslip. The dark-field scattering of the nanorod (blue curve) is strongly polarized along the nanorod longitudinal axis and is consistent with the nanorod having a larger polarizability along its long axis.[14,35,36] This angle is measured with respect to the PBD axis. In these microscopy experiments, the large numerical aperture (NA) objective produces some intensity cross-talk between the channels. This cross-talk is demonstrated in full-field electromagnetic simulations in SI Fig. S1.

We use the two-channel experiment to investigate how detuning the dye emission spectrum from the nanorod LSP spectrum affects the emission polarization from the coupled dye-nanorod system. For gold nanorods, the single-nanorod PL polarization has been found to closely resemble the dominant, longitudinal LSP mode, observed in dark-field scattering.[37,38] The fluorescence emission spectrum of the red dye Cy5.5 (Fig. 1b; solid red line) overlaps with the nanorod longitudinal LSP scattering resonance (Fig. 1b; blue line). The intensity of the longitudinal LSP mode, which peaks at 700 nm, is much stronger than transverse mode, which peaks at 560 nm (Fig. 1b; blue line). Therefore, by exciting the dye with a 635-nm laser, whose wavelength is far detuned from the nanorod LSP resonance (Fig. 1b; red arrow), we avoid fluorescence absorption enhancement to isolate the effects of coupling in the fluorescence emission. As a control experiment, similar measurements were performed with the red dye Cy3 whose emission and excitation peaks are both far detuned from the longitudinal LSP resonance (Fig. 1b; yellow lines).

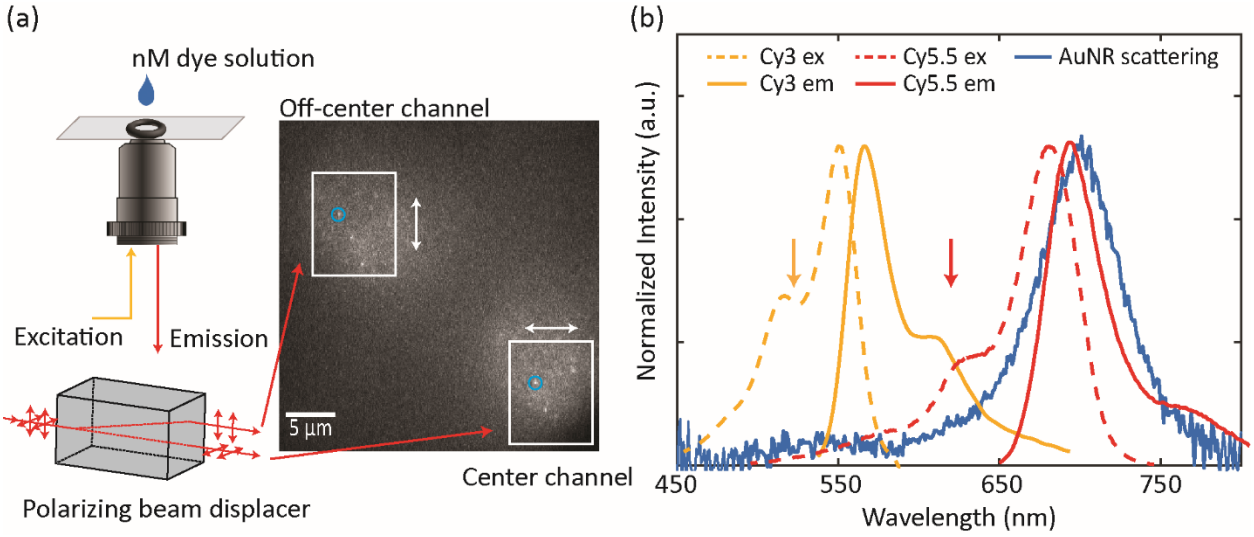

Figure 1. Experimental setup and spectral design. (a) Single-molecule polarization-resolved microscopy experiment setup. A low-concentration dye solution is excited by circularly polarized laser illumination (yellow). A polarizing beam displacer (PBD) separates the emission (red) into two orthogonally polarized output channels (white boxes; the white arrows indicate the polarization direction). The cyan circles indicate the same molecule detected in both channels. (b) Dark-field scattering spectrum of an isolated nanorod immobilized on a coverslip (blue); Cy3.5 fluorescence excitation and emission spectra (yellow dashed and solid lines, respectively); Cy5.5 fluorescence excitation and emission spectra (red dashed and solid lines, respectively). Yellow and red arrows indicate the excitation wavelengths for Cy3 and Cy5.5 respectively.

Detection of plasmon-induced emission polarization rotation from resonantly coupled dye molecules. We selected a group of seven nanorods with different orientations determined by Eq. (1) and measured the fluorescence polarization of single Cy5.5 molecules near each NR. The dark-field scattering spectra and relative angles of those nanorods are displayed in SI Fig. S2. Each system was rotated three times to sample 21 different nanorod orientations relative to the PBD axis. Simulation and model results show that molecules located more than 150 nm from the center of the nearest nanorod experience negligible mispolarization or mislocalization, and therefore these molecules experience no significant plasmonic interaction.[33] We refer to molecules located more than 400 nm from the nanorod centers as “Off-nanorod” and molecules

located within 120 nm of the nanorod centers “On-nanorod” molecules. Intermediate molecules were not considered to allow differentiation between the two populations.

For the Off-nanorod molecules, the distribution of emission polarizations measured for the Off-nanorod Cy5.5 dyes (Fig. 2a) peaks at 45°. Since the molecules adsorb non-specifically to the surface with no known favored orientation, purely *z*-oriented emitters would contribute equally in the *x* and *y* channels, leading to an artificially enhanced 45° population. Moreover, this symmetrically peaked distribution is also attributed to artifacts introduced in background-subtraction that systematically invalidate data points at low or high angles due to signal-to-noise constraints. Additionally, even in the absence of noise, the polarization cross-talk generated by the high NA objective bounds the angle domain to ~17° – 73°. A quantitative analysis of these artifacts is presented with simulated single-molecule data in SI Fig. S3. We also investigated whether this peak is due to a physical rotation of the molecules on the coverslip surface, but we found no significant time-dependent broadening of the distribution within the imaging frame integration time of the experiment, 100 ms/frame (SI Fig. S4), which supports the assumption of each molecule having a well-defined dipole moment orientation.

For the On-nanorod molecules, Fig. 2b-c shows the distributions of measured polarizations for On-nanorod Cy5.5 molecules, in which the nanorod longitudinal axis is oriented at 67° and 28°, respectively (black arrows). Though the physical orientation of the Cy5.5 molecules here is random as in the Off-nanorod case (Fig. 2a), the polarization distributions in Fig. 2b and c are shifted away from the 45° peak in Fig. 2a, and toward the nanorod orientation. The distributions of the On-nanorod Cy5.5 molecules of all 21 nanorod orientations are given in SI Fig. S5.

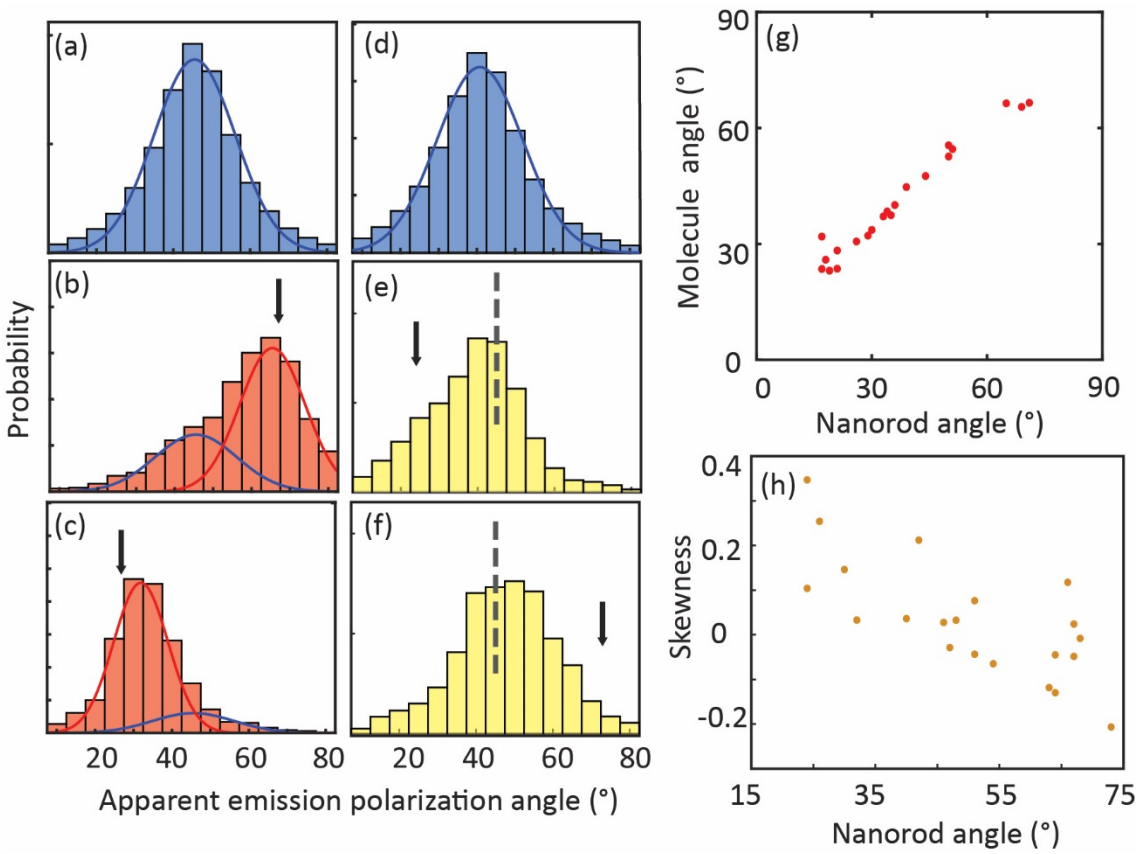

Figure 2. Characterization of Cy5.5 and Cy3 molecule apparent polarization angles, $\phi_{apparent}$. (a, d) Emission polarization angle distributions of Off-nanorod Cy5.5 and Off-nanorod Cy3 single molecules, respectively, and Gaussian curve fits. (b, c) Emission polarization angle of On-nanorod Cy5.5 single molecules. (e, f) emission polarization angle of On-nanorod Cy3 single molecules. Each histogram in (a – f) collects the apparent emission polarization angles of 2,000 – 6,000 single molecules. The black arrows in b, c, e, and f indicate the measured orientation angle of the nanorod. The vertical dashed lines in e and f indicate 45°. The histograms in b, c, e, and f are fit to the sum of two Gaussian curves: the blue one has center and width corresponding to the blue curve in a or d, and the red one is not constrained. (g) Measured Cy5.5 average polarization angles vs. nanorod orientation angle. Each point comes from the peak of a red curve as in b and c. (h) Skewness of the measured Cy3 molecule emission polarization angle distribution vs. nanorod orientation angle.

The On-nanorod distributions (Fig. 2b-c, SI Fig. S5) still include some molecules very weakly coupled to the nanorod due to the dependence of coupling both on separation and orientation.[27] To quantify the On-nanorod distribution shifts, we fit the emission polarization distribution to the sum of two Gaussian distributions: the blue curves in Fig. 2b-c, and SI Fig. S5 have center and width corresponding to the blue fit in Fig. 2a, and the red curves represent the

$\phi_{apparent}$ distribution of the truly coupled On-nanorod Cy5.5 molecules. The peak angles of these 21 red curves are compared to the nanorod longitudinal axis orientation in Fig. 2g. In Fig. 2g, it is evident that the molecular $\phi_{apparent}$ has a bias toward the nanorod longitudinal axis, in agreement with the simulation (SI Fig. S6). Furthermore, resonant coupling to the nanorod leads to an average 2-fold enhancement in PL intensity; this enhancement is greatest when $\phi_{apparent}$ is aligned with the nanorod angle (SI Fig. S7).

Polarization-sensitive detection of off-resonance molecular emission. As a control experiment, we investigated the single-molecule polarization of Cy3 molecules. Off-nanorod Cy3 molecules also appear to adsorb on the coverslip surface without preferred orientation, based on their $\phi_{apparent}$ distribution that peaks at 45° (Fig. 1d). Even in this off-resonance case, the On-nanorod polarization angle distributions are shifted away from the 45° peak (dashed lines in Fig. 1e-f) and toward the nanorod orientation (black arrows in Fig. 1e-f). For instance, the nanorod aligned at 25° in Fig. 1e shifts the distribution to the left relative to 45° and the nanorod aligned at 74° in Fig. 1f shifts the distribution to the right of 45°. The dark-field scattering spectra and relative angles of the nanorods are given in SI Fig. S8 and the full set of polarization distributions is given in SI Fig. S9. Interestingly, though the Cy3 spectrum is significantly detuned from the longitudinal LSP mode of the nanorod (Fig. 1b), the emission polarization rotates in the direction of the much stronger longitudinal mode. Still, this coupling is much weaker than that observed for the resonantly coupled Cy5.5 molecules. Thus, we characterize the shift by calculating the skewness of the polarization distributions: Fig. 2e shows a positively skewed distribution and the Fig. 2f distribution has a negative skewness. In Fig. 2h, the skewness from Cy3 emission polarization distributions for all 21 nanorod orientations is compared to the nanorod longitudinal axis orientation. There is a strong negative linear correlation between skewness and nanorod

orientation (Pearson's correlation coefficient = −0.74, p-value = 0.0001). Even in this off-resonant coupling, the longitudinal nanorod LSP mode modifies the Cy3 emission polarization. This observation is consistent with simulation (SI Fig. S10). Accordingly, no obvious fluorescence enhancement is found for On-nanorod Cy3 (SI Fig. S7).

Coupled dipole interaction model. Because the true location and orientation of individual molecules are obscured by plasmon coupling and the interference of emitted or scattered fields, current experiments are unable to relate these effects to the configuration-dependent interaction between molecule and plasmonic nanorod. We therefore turn to a simple analytical model of both the near-field interaction and far-field radiative emission to elucidate the essential details.[15,27] With the model, the effects of the nanorod longitudinal and transverse dipolar LSP modes are independently studied for molecules at specified locations and orientations. The individual influence of each mode on the observed mispolarization can then be explicitly isolated, along with its dependence on interference effects.

The fluorescence emission from the nanorod-coupled molecule is modeled as two coupled electric dipoles radiating into the far field. The governing dynamical equations for the molecule emissive transition dipole $\mathbf{p}_0$ and the induced plasmon dipole $\mathbf{p}_1$ are

$$\mathbf{p}_0 = \boldsymbol{\alpha}_0 \cdot \left(\mathbf{E}_F + \mathbf{E}_1(\mathbf{x}_0)\right), \tag{2}$$

$$\mathbf{p}_1 = \boldsymbol{\alpha}_1 \cdot \mathbf{E}_0(\mathbf{x}_1). \tag{3}$$

The orientation-dependent optical responses of the molecule and nanorod are encoded by their respective linear dyadic polarizabilities, $\boldsymbol{\alpha}_i$. The fictitious harmonic field $\mathbf{E}_F = E_0\hat{\mathbf{e}}_x e^{-i\omega t}$ drives only the molecular transition dipole, which forces both dipoles to oscillate harmonically and represents the continuous population of the molecule emissive state by absorption of the

excitation laser and subsequent fluorescence relaxation. The molecule and plasmon are coupled by the fully retarded dipole fields, $\mathbf{E}_i(\mathbf{x}_j) = \mathbf{G}(\mathbf{x}_j, \mathbf{x}_i) \cdot \mathbf{p}_i$, generated by the *i*th dipole evaluated at the location of the *j*th dipole; here $\mathbf{G}$ is the standard electric dipole relay tensor (Supplementary Note 1).[39] Upon substituting $\mathbf{E}_i(\mathbf{x}_j)$ for the dipole fields in Eqs. (2) and (3), the coupled equations can be solved to yield the complex dipole moments containing both oscillation magnitude and phase as functions of the polarizabilities and dipole-dipole orientation (Supplementary Note 1 and SI Fig. S17).

With an analytical relationship between the two dipole moments, the dyadic polarizabilities can be parameterized from spectra of the uncoupled molecules and nanorod. For this purpose, the molecule emissive dipole transition is modeled by a Lorentz oscillator polarizable only in one direction fixed by the molecular orientation; i.e., $\boldsymbol{\alpha}_0 = \hat{\mathbf{e}}_x \alpha_{\mathrm{mol}} \hat{\mathbf{e}}_x$ in the reference frame of the molecule. The nanorod is approximated as a prolate spheroid in the modified long-wavelength approximation,[40] with polarizability $\boldsymbol{\alpha}_1 = \hat{\mathbf{e}}_{x'} \alpha_{\mathrm{short}} \hat{\mathbf{e}}_{x'} + \hat{\mathbf{e}}_{y'} \alpha_{\mathrm{long}} \hat{\mathbf{e}}_{y'} + \hat{\mathbf{e}}_{z'} \alpha_{\mathrm{short}} \hat{\mathbf{e}}_{z'}$ in the basis aligned with the nanorod principal axes. The prolate spheroid geometry idealizes the true nanorod geometry to allow for a closed form solution to Maxwell's equations including radiation damping for the dipolar LSPs. Both components of $\boldsymbol{\alpha}_1$ are parameterized by the two unique semi-radii of the cylindrical nanorod (here 44 nm and 20 nm) and three material parameters built into the Drude model dielectric function describing the electronic responses of bulk gold (Supplementary Note 2 and SI Fig. S17).

To compute the two-channel diffraction-limited images generated by the PBD, the fields emitted by the coupled dipoles in Eq. (2) and (3) are propagated through an idealized microscope. The resulting image contains the superposition of the focused and diffraction-

limited fields, $\mathbf{E}_0^{\mathrm{im}}$ and $\mathbf{E}_1^{\mathrm{im}}$, which are proportional to each dipole moment respectively (Supplementary Note 3). In accordance with our experiment, orthogonal polarization components of the total field are split to form separate images, each with the form:

$$I_q = \frac{cn}{8\pi}\left(\left|\mathbf{E}_0^{\mathrm{im}} \cdot \hat{\mathbf{e}}_q\right|^2 + \left|\mathbf{E}_1^{\mathrm{im}} \cdot \hat{\mathbf{e}}_q\right|^2 + 2\,Re[\mathbf{E}_0^{\mathrm{im}} \cdot \hat{\mathbf{e}}_q\ \mathbf{E}_1^{\mathrm{im}} \cdot \hat{\mathbf{e}}_q]\right), \tag{4}$$

where $q \in \{x, y\}$ are analogous to the center and off-center experimental image channels, c is the speed of light in vacuum, and n is the refractive index of the background medium (here water). Combining this polarized image intensity with Eq. (1) makes explicit how the average emission polarization measured in experiment is determined by the orientation-dependent relay tensor $\mathbf{G}$ that influences the dipole moment magnitudes and phases according to Eqs. (2) and (3). The polarizabilities in the latter equations are parametrized from the independent dye emission and nanorod scattering spectra. By assuming the nanorod location and orientation are determined, Eq. (4) provides an analytical measure of the imaged intensities and observed polarization as a function of molecule position and orientation.

Analysis of the isolated contributions from the transverse and longitudinal LSP modes and interference. By manually setting the short- or long-axis components of the nanorod polarizability to zero in the model, the independent contributions of the transverse and longitudinal LSP modes on ϕ_{apparent} can be studied. As in the experiments, ϕ_{apparent} (Eq. (1)) maps onto an angle range slightly smaller than 0 – 90° due to the inherent cross-talk. In both the analytical model and the simulations, the calculated polarization is mapped back onto a 0 – 90° range by inverting the one-to-one mapping between the true dipole orientation in plane and ϕ_{apparent} (SI Fig. S1). To determine how interference affects the PBD-resolved emission polarization[16], we also compare the full emission polarization with that produced by the isolated

plasmon modes in the absence of the interference term in Eq. (4). Four geometries are studied: 0°-oriented molecular dipoles analogous to Cy5.5 (i.e., parallel to and resonant with the longitudinal LSP mode), 0°-oriented molecular dipoles analogous to Cy3 (i.e., parallel to and off resonance with the longitudinal LSP mode), 90°-oriented dipoles analogous to Cy5.5 (i.e., perpendicular to and resonant with the longitudinal LSP mode), and 90°-oriented dipoles analogous to Cy3 (i.e., perpendicular to and off resonance with the longitudinal LSP mode); SI Figs. S11 – S14.

The most significant mispolarization is shown in the configuration of the 0°-oriented molecular dipoles resonant with the longitudinal LSP (Fig. 3a). Fig. 4b-c shows the decomposition of the ϕ_{apparent} of these molecules by projecting onto either the transverse or longitudinal LSP modes in isolation. Comparing among the panels in Fig. 3, it is clear that the experimentally measured skew of molecule emission polarization toward the nanorod long axis displayed in Fig. 2 is mostly due to superposition of the longitudinal plasmon mode scattering with the molecular emission. Molecules not aligned with the main nanorod axis still couple to and drive the long-axis dipole plasmon, which emits mostly light polarized along its axis and biases the average polarization across an image in its favor. However, similar polarization maps for 90°-oriented dipoles resonant with the longitudinal LSP (Fig. 3d-i) show that the influence of the longitudinal LSP upon ϕ_{apparent} is more complicated: as in the case for 0° orientation, the longitudinal LSP strongly mispolarizes the molecular emission toward the longitudinal LSP mode (aligned along the *y*-axis) by superposition with fluorescence emission redirected through the plasmon (Fig. 3d-f); additionally, for the 90° case, the longitudinal LSP mode mispolarizes dipoles that are parallel to *y*-axis toward the transverse mode axis (aligned along the *x*-axis) orientation because of destructive interference effects in the *y*-oriented fields (Fig. 3g-i). This

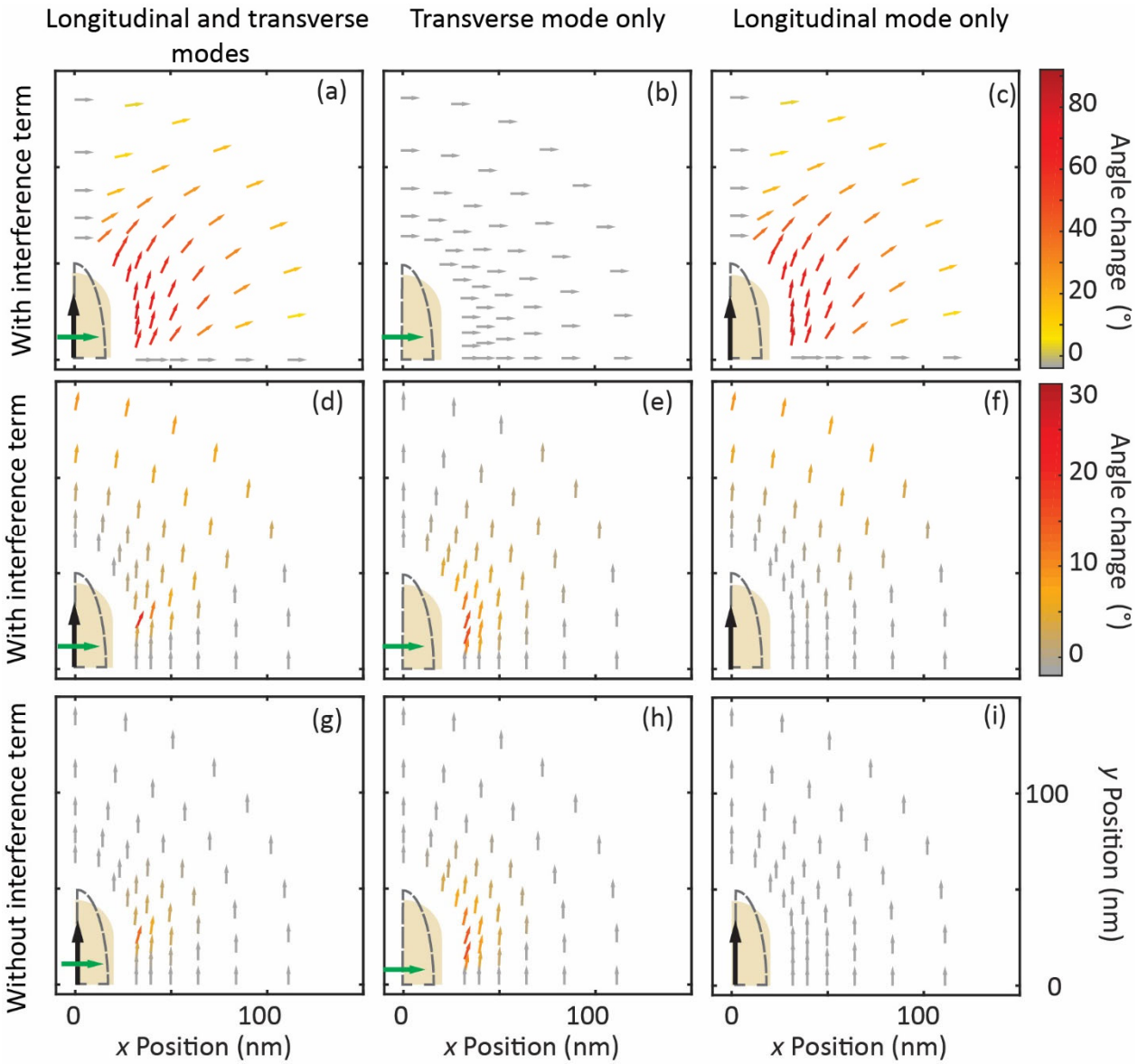

Figure 3. Mispolarization map calculated from the coupled-dipole model. (a) – (c) $\phi_{apparent}$ maps corresponding to 0°-oriented molecular dipoles resonant with the longitudinal LSP. (d) – (i) $\phi_{apparent}$ maps corresponding to 90°-oriented molecular dipoles that are also resonant with the longitudinal LSP. The black and green arrows indicate the longitudinal and transverse LSP modes, respectively, of the nanorod. The tan shapes in (a) – (i) represent a quarter of the simulated nanorod. The black dashed outline represents the prolate spheroid model of the nanorod (best fit geometric and material parameters are given in Supplementary Note 2).

interference effect results from the far-fields of the molecule and nanorod that are parallel to their dipole moments being out of phase, thereby turning the last term in Eq. (4) negative for both components, which reduces the argument of the arctangent in Eq. (1) and therefore reduces the observed polarization angle below 90°. The transverse plasmon mode produces mispolarization of 90° molecules close in proximity to its dipole moment by superposition similar to how the longitudinal mode mispolarizes *x*-oriented molecules. However, as the electric field of the transverse LSP mode is much weaker than that of the longitudinal mode, the transverse mode does not change the polarization as much as the longitudinal mode even for resonant molecules (SI Fig. S13).

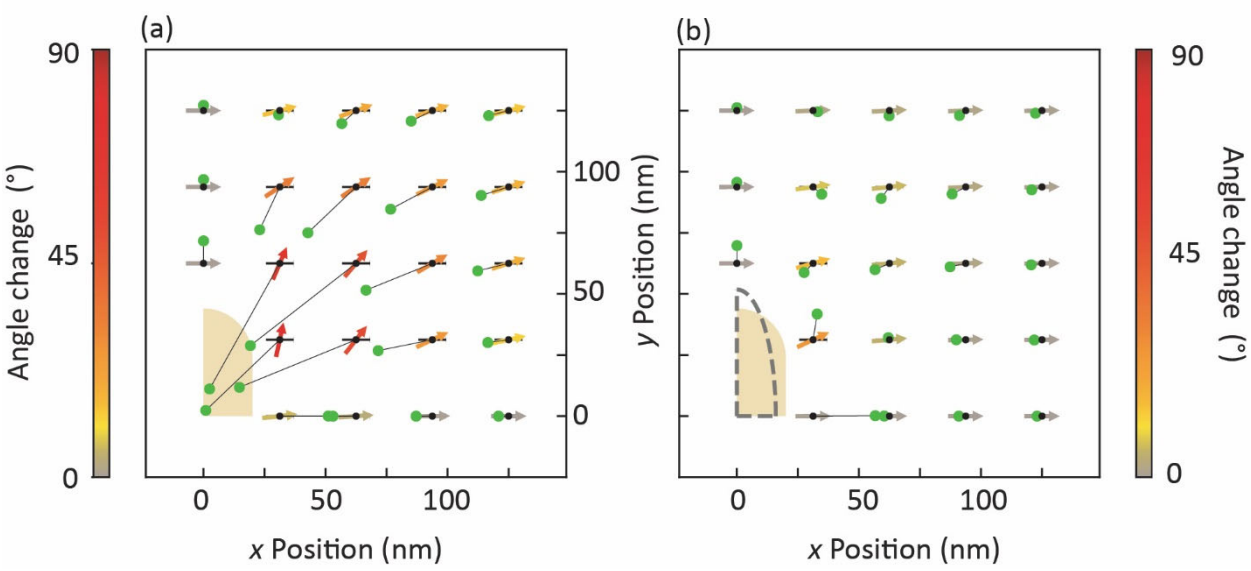

Figure 4. Comparison of the best fit results for dipole position (green) and polarization (colored arrows) determined in simulated diffraction-limited images (at a single frequency matching the longitudinal LSP peak in SI Fig. S18) of 23 simulated single-molecule dipoles (black dots) oriented parallel to the x-axis and placed near a nanorod (shaded tan) up to 150 nm away from the center of the nanorod. (a) Gaussian localization of the total intensity paired with molecule orientation as would be determined by polarization-resolved microscopy reveals the familiar mislocalization of *x*-oriented molecules mostly toward the nanorod (apparent locations marked by green dots connected to the true molecule location in black) is accompanied by mispolarization of the molecules due to superposition of fluorescence emission redirected through the nanorod. (b) Least-squares fit of the model-generated images to simulated images.

Model fit for extraction of molecule polarization and location. Previous work demonstrated that plasmon-induced deformation of single-molecule fluorescence produces a difference between the true and apparent single-molecule position[27] and polarization.[21,23,25] Here, we measure single-molecule polarization with high-throughput experiments and demonstrate how to model the observable ϕ_{apparent} analytically. The model-generated image (Eq. (4)) can also be used as a simultaneous localization and polarization fit function to recover the true position and orientation of nanorod-coupled dye molecules. Fig. 4 compares the accuracy of molecular polarization and location determined by a least-squares model fit to simulated images (Fig. 4b) with that determined by the PBD and typical Gaussian fitting (Fig. 4a). The molecules in Fig. 4 are aligned along the *x*-axis (0°); other geometries are considered in Supplementary Note 3 and SI Figs. S19 – S21. For the model fits in Fig. 4b, the molecule and nanorod dipoles are parametrized, leaving only three fit parameters for residual minimization: the *x* and *y* coordinates of the molecular transition dipole relative to the center of the nanorod, and the dipole angle.

The model-based localization and polarization significantly outperforms Gaussian localization and effectively eliminates the mispolarization observed in ϕ_{apparent} for all molecules studied here except those closest to the nanorod corner. The mislocalization error is greatly reduced because, unlike Gaussian fitting, the molecule location is estimated with full knowledge of the interaction and configuration-dependent far-field radiation pattern produced by coupled dipoles. Any error left in the determined molecule location is not due to convolution of molecule and nanorod emission, but is likely a due to the slight deficiency of the Drude model dielectric function for describing the optical response of gold in the frequency range spanning the longitudinal and transverse mode resonances (SI Fig. S18). Although a model dielectric function with greater predictive power and more fit parameters can easily be employed, the degree of

success achieved here demonstrates that the relevant physics underlying the diffraction-limited image of coupled molecule and nanorod can be qualitatively captured with only the three Drude material parameters.

The in-plane molecule orientation is determined by the model fit in a qualitatively different manner from the way ϕ_{apparent} is calculated. While the latter is a measure of the average polarization of a dye molecule in the focused image field, the model fit angle is a direct estimation of the orientation of the molecule emissive transition dipole moment during the time span of photon collection. At close molecule-nanorod separations, the localization provided by the model fit seems to be no more reliable than Gaussian fitting. This fitting error is due to the simplicity of the model rather than the fitting process. For instance, greater accuracy could be achieved by including the nanorod quadrupolar LSP response which becomes increasingly important at close proximity.

In conclusion, using high-throughput single-molecule polarization-resolved microscopy, we have discovered that emission polarization is a measure of the coupling strength between molecular emitters and plasmonic nanoantennas. The stronger the coupling of the molecule to a plasmonic nanoantenna, the more the molecule emission polarization will rotate toward the polarization of the nanoantenna LSP mode. While this effect is apparent for an ensemble of single molecule measurements, simulations and analytical modeling demonstrate that the mispolarization of single molecules with known location and orientation is much more complicated. ϕ_{apparent} is rotated both toward and away from the nanorod long-axis by two distinct physical phenomena, even for molecules that are resonant with the nanorod longitudinal LSP mode. Either constructive or destructive interference can dominate depending on the molecule orientation and location relative to the nanorod.

Significantly, the emission polarization is a more sensitive measure of coupling than fluorescent intensity enhancement because, even for weakly coupled Cy3 where no apparent fluorescent enhancement is observed, the emission polarization change is appreciable. The complex relationship between ϕ_{apparent} and the configuration-dependent electromagnetic interaction between molecule and nanorod facilitates simultaneous extraction of molecule orientation and location by fitting an analytical model of the coupled-dipole image to experimental data. The model developed exceeds the accuracy of the best fits achieved through standard Gaussian localization as well as PBD-based determination of the in-plane polarization angle for simulated molecule-nanorod images. Future work will use this model fit to extract the true molecule location and orientation from experimental images.

Associated Content

The Supporting Information is available free of charge on the ACS Publications website at DOI: …

Details of the experimental and computational methods, description of experimental corrections, dark field scattering spectra of the nanorods, measured emission polarization angle distributions of all Cy5.5 and Cy3 molecules, simulated apparent emission polarization distributions, single-molecule fluorescence enhancement measurements, apparent emission polarizations from electrodynamics simulations at the Cy3 and Cy5.5 wavelengths and in two orthogonal directions, detailed description of the analytical model: the two coupled dipole model, the polarizability, and the diffraction-limited dipole image fields, supplementary references.

Acknowledgements

The experiments and simulations were supported by a NSF Award CHE-1807676 to JSB. Theoretical modeling of the coupled emitter-nanoantenna system was supported by NSF Award CHE-1664684 to DJM and the modeling of the collection optics and far-field signal was supported by NSF CHE-1727092 to DJM.

Author Contributions

TZ designed and carried out the experiments, analyzed data, and performed time-domain electromagnetic simulations with help from JSB. HJG developed and implemented the analytical model and performed frequency-domain electromagnetic simulations with help from DJM. BPI set up the time-domain electromagnetic simulations. TZ and HJG wrote the paper. All authors discussed the results and analysis, developed conclusions, and edited the paper.

References

1. Novotny, L.; van Hulst, N. Antennas for Light. *Nature Photon.* **2011***, 5,* 83-90.

2. Anker, J. N.; Hall, W. P.; Lyandres, O.; Shah, N. C.; Zhao, J.; Van Duyne, R. P. Biosensing with Plasmonic Nanosensors. *Nature Mater.* **2008***, 7,* 442-453.

3. Doria, G.; Conde, J.; Veigas, B.; Giestas, L.; Almeida, C.; Assunção, M.; Rosa, J.; Baptista, P. V. Noble Metal Nanoparticles for Biosensing Applications. *Sensors* **2012***, 12,* 1657-1687.

4. Ozbay, E. Plasmonics: Merging Photonics and Electronics at Nanoscale Dimensions. *Science* **2006***, 311,* 189-193.

5. Brolo, A. G. Plasmonics for Future Biosensors. *Nat. Photon.* **2012***, 6,* 709-713.

6. Nie, S.; Emory, S. R. Probing Single Molecules and Single Nanoparticles by Surface-Enhanced Raman Scattering. *Science* **1997***, 275,* 1102-1106.

7. Cialla, D.; März, A.; Böhme, R.; Theil, F.; Weber, K.; Schmitt, M.; Popp, J. Surface-Enhanced Raman Spectroscopy (SERS): Progress and Trends. *Anal. Bioanal. Chem.* **2012***, 403,* 27-54.

8. Yuan, H.; Khatua, S.; Zijlstra, P.; Yorulmaz, M.; Orrit, M. Thousand-Fold Enhancement of Single-Molecule Fluorescence Near a Single Gold Nanorod. *Angew. Chem., Int. Ed.* **2013***, 52,* 1217-1221.

9. Akselrod, G. M.; Argyropoulos, C.; Hoang, T. B.; Ciracì, C.; Fang, C.; Huang, J.; Smith, D. R.; Mikkelsen, M. H. Probing the Mechanisms of Large Purcell Enhancement in Plasmonic Nanoantennas. *Nat. Photon.* **2014***, 8,* 835-840.

10. Willets, K. A.; Wilson, A. J.; Sundaresan, V.; Joshi, P. B. Super-Resolution Imaging and Plasmonics. *Chem. Rev.* **2017***, 117,* 7538-7582.

11. Biteen, J.; Willets, K. A. Introduction: Super-Resolution and Single-Molecule Imaging. *Chem. Rev.* **2017***, 117,* 7241-7243.

12. Kinkhabwala, A.; Yu, Z.; Fan, S.; Avlasevich, Y.; Mullen, K.; Moerner, W. E. Large Single-Molecule Fluorescence Enhancements Produced by a Gold Bowtie Nanoantenna. *Nat. Photon.* **2009***, 3,* 654-657.

13. Bharadwaj, P.; Novotny, L. Spectral Dependence of Single Molecule Fluorescence Enhancement. *Opt. Express* **2007***, 15,* 14266-14274.

14. Ringler, M.; Schwemer, A.; Wunderlich, M.; Nichtl, A.; Kuerzinger, K.; Klar, T. A.; Feldmann, J. Shaping Emission Spectra of Fluorescent Molecules with Single Plasmonic Nanoresonators. *Phys. Rev. Lett.* **2008***, 100,* 203002.

15. Ayala-Orozco, C.; Liu, J. G.; Knight, M. W.; Wang, Y.; Day, J. K.; Nordlander, P.; Halas, N. J. Fluorescence Enhancement of Molecules Inside a Gold Nanomatryoshka. *Nano Lett.* **2014***, 14,* 2926-2933.

16. Pelton, M. Modified Spontaneous Emission in Nanophotonic Structures. *Nat. Photon.* **2015***, 9,* 427-435.

17. Anger, P.; Bharadwaj, P.; Novotny, L. Enhancement and Quenching of Single-Molecule Fluorescence. *Phys. Rev. Lett.* **2006***, 96,* 113002.

18. Boutelle, R. C.; Neuhauser, D.; Weiss, S. Far-Field Super-Resolution Detection of Plasmonic Near-Fields. *ACS Nano* **2016***, 10,* 7955-7962.

19. Ropp, C.; Cummins, Z.; Nah, S.; Fourkas, J. T.; Shapiro, B.; Waks, E. Nanoscale Probing of Image-Dipole Interactions in a Metallic Nanostructure. *Nat. Commun.* **2015***, 6,* 6558.

20. Moerland, R. J.; Taminiau, T. H.; Novotny, L.; van Hulst, N. F.; Kuipers, L. Reversible Polarization Control of Single Photon Emission. *Nano Lett.* **2008***, 8,* 606-610.

21. Taminiau, T. H.; Stefani, F. D.; van Hulst, N. F. Enhanced Directional Excitation and Emission of Single Emitters by a Nano-Optical Yagi-Uda Antenna. *Opt. Express* **2008***, 16,* 10858-10866.

22. Taminiau, T. H.; Stefani, F. D.; Segerink, F. B.; van Hulst, N. Optical Antennas Direct Single-Molecule Emission. *Nat. Photon.* **2008***, 2,* 234-237.

23. Shegai, T.; Li, Z.; Dadosh, T.; Zhang, Z.; Xu, H.; Haran, G. Managing Light Polarization Via Plasmonics Molecule Interactions within an Asymmetric Metal Nanoparticle Trimer. *Proc. Natl. Acad. Sci. USA* **2008***, 105,* 16448.

24. Curto, A. G.; Volpe, G.; Taminiau, T. H.; Kreuzer, M. P.; Quidant, R.; van Hulst, N. F. Unidirectional Emission of a Quantum Dot Coupled to a Nanoantenna. *Science* **2010***, 329,* 930-933.

25. Ren, M.; Chen, M.; Wu, W.; Zhang, L.; Liu, J.; Pi, B.; Zhang, X.; Li, Q.; Fan, S.; Xu, J. Linearly Polarized Light Emission from Quantum Dots with Plasmonic Nanoantenna Arrays. *Nano Lett.* **2015***, 15,* 2951-2957.

26. Wertz, E. A.; Isaacoff, B. P.; Biteen, J. S. Wavelength-Dependent Super-Resolution Images of Dye Molecules Coupled to Plasmonic Nanotriangles. *ACS Photonics* **2016***, 3,* 1733-1740.

27. Goldwyn, H. J.; Smith, K. C.; Busche, J. A.; Masiello, D. J. Mislocalization in Plasmon-Enhanced Single-Molecule Fluorescence Microscopy as a Dynamical Young's Interferometer. *ACS Photonics* **2018***, 5,* 3141-3151.

28. Khatua, S.; Paulo, P. M. R.; Yuan, H.; Gupta, A.; Zijlstra, P.; Orrit, M. Resonant Plasmonic Enhancement of Single-Molecule Fluorescence by Individual Gold Nanorods. *ACS Nano* **2014***, 8,* 4440-4449.

29. Mack, D.; Cortés, E.; Giannini, V.; Török, P.; Roschuk, T.; Maier, S. Decoupling Absorption and Emission Processes in Super-Resolution Localization of Emitters in a Plasmonic Hotspot. *Nat. Commun.* **2017***, 8,* 14513.

30. Mertens, H.; Polman, A.; Biteen, J. S.; Atwater, H. A. Polarization-Selective Plasmon-Enhanced Silicon Quantum Dot Luminescence. *Nano Lett.* **2006***, 6,* 2622-2625.

31. Sharonov, A.; Hochstrasser, R. M. Wide-Field Subdiffraction Imaging by Accumulated Binding of Diffusing Probes. *Proc. Natl. Acad. Sci. U. S. A.* **2006***, 103,* 18911-18916.

32. Fu, B.; Isaacoff, B. P.; Biteen, J. S. Super-Resolving the Actual Position of Single Fluorescent Molecules Coupled to a Plasmonic Nanoantenna. *ACS Nano* **2017***, 11,* 8978-8987.

33. Fu, B.; Flynn, J. D.; Isaacoff, B. P.; Rowland, D. J.; Biteen, J. S. Super-Resolving the Distance-Dependent Plasmon-Enhanced Fluorescence of Single Dye and Fluorescent Protein Molecules. *J. Phys. Chem. C* **2015***, 119,* 19350-19358.

34. Isaacoff, B. P.; Li, Y.; Lee, S. A.; Biteen, J. S. SMALL-LABS: An Algorithm of Measuring Single-Molecule Intensity and Position in the Presence of Obscuring Backgrounds. *Biophys. J.* **2019***, 116,* 975-982.

35. Sönnichsen, C.; Franzl, T.; Wilk, T.; von Plessen, G.; Feldmann, J.; Wilson, O.; Mulvaney, P. Drastic Reduction of Plasmon Damping in Gold Nanorods. *Phys. Rev. Lett.* **2002***, 88,* 077402.

36. Sönnichsen, C.; Alivisatos, A. P. Gold Nanorods as Novel Nonbleaching Plasmon-Based Orientation Sensors for Polarized Single-Particle Microscopy. *Nano Lett.* **2005***, 5,* 301-304.

37. Fang, Y.; Chang, W.; Willingham, B.; Swanglap, P.; Dominguez-Medina, S.; Link, S. Plasmon Emission Quantum Yield of Single Gold Nanorods as a Function of Aspect Ratio. *ACS Nano* **2012***, 6,* 7177-7184.

38. Cai, Y.; Liu, J. G.; Tauzin, L. J.; Huang, D.; Sung, E.; Zhang, H.; Joplin, A.; Chang, W.; Nordlander, P.; Link, S. Photoluminescence of Gold Nanorods: Purcell Effect Enhanced Emission from Hot Carriers. *ACS Nano* **2018***, 12,* 976-985.

39. Novotny, L.; Hecht, B. *Principles of Nano-Optics*; Cambridge University Press: Cambridge, UK, 2006.

40. Bohren, C. F.; Huffman, D. R. *Absorption and Scattering of Light by Small Particles;* Wiley: New York, 1983.